ELSEVIER

Journal of Alloys and Compounds 234 (1996) 1–5

Journal of ALLOYS AND COMPOUNDS

Phase stabilities of $LnMn_2O_5$ (Ln = rare earth)

H. Satoh, S. Suzuki, K. Yamamoto, N. Kamegashira

Department of Materials Science, Toyohashi University of Technology, Tempaku-cho, Toyohashi 441, Japan

Received 23 March 1995; in final form 12 May 1995

Abstract

Decomposition temperatures of $LnMn_2O_5$ (Ln = Pr, Nd, Sm, Eu, Gd, Tb, Dy, Ho, Er, Tm, Yb and Y) were measured by thermogravimetry (TG) and differential thermal analysis under various oxygen partial pressures $P_{O_2} = 10^{-4}$–1 atm. The decomposition reactions were confirmed by identifying the decomposition products with powder X-ray diffractometry and determining weight loss from TG as follows.

$$LnMn_2O_5 \rightarrow LnMnO_3 + \tfrac{1}{3}Mn_3O_4 + \tfrac{1}{3}O_2$$

Among $LnMn_2O_5$ phases the most stable phases are $GdMn_2O_5$ and $DyMn_2O_5$, while the most unstable phase is $PrMn_2O_5$. The Gibbs free energy, enthalpy and entropy changes of the decomposition reactions for $LnMn_2O_5$ phase were determined from the oxygen partial pressure at the decomposition temperature. The standard enthalpies and entropies of formation of $LnMn_2O_5$ were estimated

Keywords: Manganite; Thermodynamics; Oxygen partial pressure

1. Introduction

$LnMn_2O_5$ compounds were first synthesized by Quezel-Ambrunaz et al. [1] and isostructural $LnMTiO_5$ (M = Cr, Mn, Fe) phases were also reported [2–4]. The crystal structure [5–7], magnetic structure at low temperature [2,3,8,9] and dielectric properties [10] of $LnMn_2O_5$ and $LnMnTiO_5$ have been investigated. Recently, single crystals of $NdMn_2O_5$ with good quality were prepared by Euzen et al. [11] using a redox reaction of MnO_2 and $NdCl_3$ and the crystal structure was resolved. According to them, $NdMn_2O_5$ has the orthorhombic structure of *Pbam*, analogous to the $BiMn_2O_5$ structure [12]. Both of these compounds contain Mn^{3+} and Mn^{4+} ions. The Mn^{3+} ions located in a pyramid of five oxygen ions and slightly shifted in the pyramid from the centre of the square. A sixth oxygen ion is rather too far away to be regarded as ligand of the Mn ion. The Mn^{4+} ion is located in an almost undistorted oxygen octahedron. The Ln^{3+} ion is located non-centrally in a polyhedron which consists of eight oxygen ions.

Thermodynamic properties of $LnMn_2O_5$ were recently studied for Ln = Pr and Nd using e.m.f. measurements in a galvanic cell with solid electrolytes by Cherepanov et al. [13]. However, the thermodynamic properties of $LnMn_2O_5$ compounds with other rare earth were not reported. Although thermodynamic data of $LnMnO_3$ were collected into MALT2 [14], those of $LnMn_2O_5$ and another compounds of rare earth manganites [15–18] are rather limited. In this paper a study of the thermodynamic stability of $LnMn_2O_5$ phase is described.

2. Experimental details

The formation of $LnMn_2O_5$ was difficult by the usual ceramic method. Buisson [2,12] tried to prepare YMn_2O_5 from a mixture of yttrium and manganese oxides but this led to only the formation of $YMnO_3$. The formation of YMn_2O_5 could be realized only by heating the nitrate solution [12]. In our experiment all attempts to form $LnMn_2O_5$ phases by heating a mixture of rare earth and manganese oxides were unsuccessful. So two methods were tried to obtain $LnMn_2O_5$ phases. Ln_2O_3 (99.99% in purity, Rare Metallic Co. Ltd.) and metallic Mn (99.9%, Rare Metallic Co. Ltd.) were used as staring materials. Ln_2O_3 was heated at 1273 K in Ar (H_2 in the cases of

SSDI 0925-8388(95)01881-6

Table 1
Lattice parameters of $LnMn_2O_5$

Specimen	Lattice parameters			
	a(nm)	b (nm)	c (nm)	V (nm^3)
$PrMn_2O_5$	0.752(1)	0.863(1)	0.571(1)	0.370
$NdMn_2O_5$	0.7499(9)	0.861(1)	0.5717(7)	0.369
$SmMn_2O_5$	0.7445(6)	0.8585(7)	0.568(4)	0.363
$EuMn_2O_5$	0.741(1)	0.856(1)	0.572(1)	0.363
$GdMn_2O_5$	0.7337(1)	0.8536(2)	0.5683(1)	0.357
$TbMn_2O_5$	0.7278(2)	0.8492(3)	0.5676(2)	0.351
$DyMn_2O_5$	0.7300(3)	0.8482(4)	0.5674(3)	0.351
$HoMn_2O_5$	0.731(1)	0.849(1)	0.567(1)	0.353
$ErMn_2O_5$	0.7274(7)	0.8461(9)	0.5672(6)	0.349
$TmMn_2O_5$	0.7222(8)	0.8431(9)	0.5655(6)	0.344
$YbMn_2O_5$	0.7207(5)	0.8400(6)	0.5638(4)	0.341
YMn_2O_5	0.7259(8)	0.8456(9)	0.569(6)	0.349

Numbers in parentheses indicate the estimated standard deviation of the last significant digit.

Pr and Tb) for 24 h and metallic Mn was washed sequentially in dilute HCl, pure water and methanol or acetone. After such pretreatment, these starting materials in an appropriate ratio were dissolved into HNO_3 solution. The solution was dried and heated to 873 K to decompose nitrate. The residual powders were ground and then pressed into a pellets. The pellets were heated at 1373 K for 48 h in air or oxygen flow. If a single phase could not be obtained, the process was repeated at a lower temperature. Some of the samples were also synthesized by the decomposition of mixed 2-ethylhexanoates of rare earth and manganese. Each complex of 2-ethylhexanoate was prepared by the same method as previously reported [19] and heated to 1273 K. The same results were obtained, regardless of the method of preparation. The final products were identified by powder X-ray diffractometry (Geigerflex-2000, Rigaku Ltd.). The lattice parameters of $LnMn_2O_5$ are shown in Table 1 and are in good agreements with those of Refs. [1,4,6].

The thermogravimetry–differential thermal analysis (TG–DTA) apparatus was used with a model TG/DTA-200 apparatus of Seiko Electronic Industry Co. Ltd. A mixture of Ar and O_2 gases was used for generating various oxygen partial pressures. The flow rate of gas was about 100 ml min^{-1} and the heating rate was 2 K min^{-1}. TG and DTA were measured from 900 K to 1623 K under each oxygen partial pressure ($P_{O_2} = 10^4$–1 atm). The decomposition products were determined from the powder X-ray diffractometry of decomposed phases and the weight loss of TG measurement.

3. Results and discussion

The decomposition temperature of Co_3O_4 (99.9% purity, Rare Metallic Co. Ltd.) was measured under the same conditions in order to check the accuracy of the present measurement. The results are shown in Fig. 1. If the slope and the intercept of the line in Fig. 1 are written as A and B respectively, the equation of the line is expressed as follows:

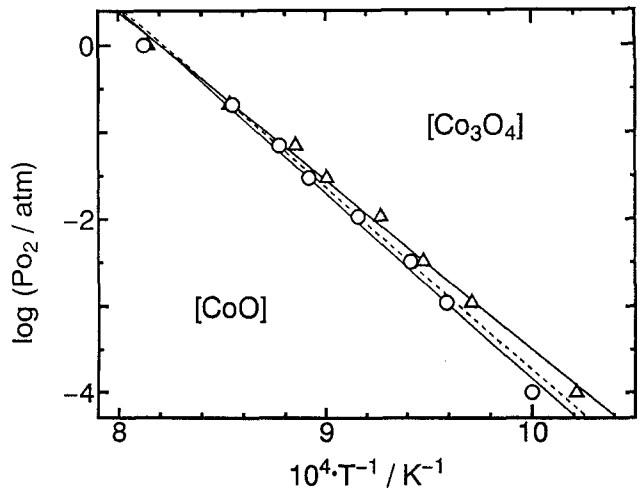

Fig. 1. Decomposition oxygen partial pressure vs. reciprocal temperature for Co_3O_4 ($\log P_{O_2}$–$1/T$ phase diagram): ○, decomposition points read out from DTA; △, results from TG; ——, results of least-squares method for TG and DTA data; – – –, results from JANAF [20].

$$\log P_{O_2} = -\frac{A}{T} + B \quad (1)$$

The decomposition reaction of Co_3O_4 is already known as

$$Co_3O_4 \rightarrow 3CoO + \tfrac{1}{2}O_2 \quad (2)$$

Hence the Gibbs free energy change and oxygen partial pressure of the decomposition are connected by the following equation:

$$\Delta G^\circ_T = -RT \ln P^{1/2}_{O_2} \quad (3)$$

Substituting Eq. (1) into (3) and rearranging, the enthalpy and entropy changes for the reaction (2) can be obtained.

The results at the mean temperature are tabulated in Table 2 with the values at those temperature calculated from JANAF tables [20]. By comparison of the present DTA data with JANAF results, the deviations in accuracy of enthalpy and entropy changes were each within 2%. On the contrary, those of TG were −7% and −8% respectively. Hence, enthalpy and entropy changes estimated from DTA are in good agreement with the calculated values from JANAF tables. As it is considered that the results from DTA have higher accuracy, TG measurement was carried out only to check the weight loss.

TG and DTA measurements were performed for $LnMn_2O_5$. From the weight loss with TG and identifi-

Table 2
Coefficients A and B of Eq. (1) calculated from differential thermal analysis and enthalpy and entropy changes at the mean temperature for decomposition of Co_3O_4 with the corresponding data of JANAF [20]

	A ($\times 10^4$ K^{-1})	B	T_{mean} (K)	$\Delta H°$ (kJ mol^{-1})	$\Delta S°$ (J mol^{-1} K^{-1})
TG	1.944	15.94	1104	186.1	152.6
DTA	2.135	17.51	1116	204.4	167.6
JANAF			1104	201.0	165.2
			1116	200.5	164.8

cation of phases by X-ray diffractometry for the decomposed residues, the decomposition reactions were confirmed as follows for each rare earth:

$$LnMn_2O_5 \rightarrow LnMnO_3 + \tfrac{1}{3}Mn_3O_4 + \tfrac{1}{3}O_2 \quad (4)$$

From Pr to Dy, $LnMnO_3$ has an orthorhombically distorted perovskite structure. On the contrary, from Ho to Yb and Y, $LnMnO_3$ normally has a hexagonal structure which is different from the perovskite-type structure. The variation in decomposition temperature of $LnMn_2O_5$ in air with ionic radius of the rare earth is plotted in Fig. 2. The decomposition temperatures for reaction (4) in air were determined by the present measurement to be 1355 K and 1383 K for $PrMn_2O_5$ and $NdMn_2O_5$ respectively. These temperatures correspond to 1367 K and 1360 K respectively obtained by Cherepanov et al. [13]. From this figure, the most stable phases are $GdMn_2O_5$ and $DyMn_2O_5$, and the most unstable phase is $PrMn_2O_5$ in air. As described previously, the boundary between the two different structures for $LnMnO_3$ is between Dy and Ho. It is noted that these compounds have the maximum temperature for stability in air as is shown in Fig. 2. The phase diagrams of $\log P_{O_2} = 1/T$ for these compounds

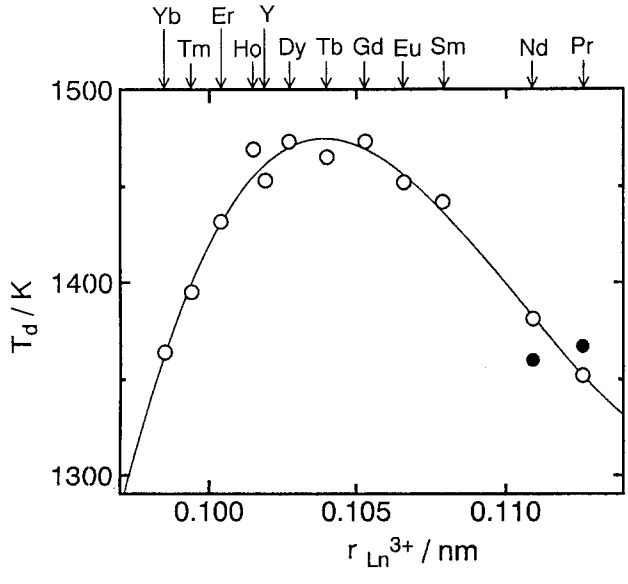

Fig. 2. Dependence of decomposition temperature on ionic radius for rare earths in air from DTA: ○, this study; ●, from Cherepanov et al. [13].

are shown in Fig. 3. The results for $PrMn_2O_5$ obtained by Cherepanov et al. [13] are also shown in Fig. 3. In this figure the present results have slightly higher slopes than those of Cherepanov et al. [13]. The difference $\Delta\log(P_{O_2}/\text{atm})$ in oxygen partial pressure is 0.5 at 1273 K under the low oxygen partial pressure region. The e.m.f. method is an absolute measurement, but the present method (DTA) is a dynamic measurement and the true equilibrium of Eq. (4) is rather difficult to realize by this method, although a slow heating rate would approach the equilibrium. In particular, under low oxygen partial pressure the diffusion rate in the $LnMn_2O_5$ phase may be low, which is one of the reason that it is very difficult to synthesize these phases by the solid state reaction as mentioned above. It is seen from these figures that the boundary lines of each phase are approximately parallel. With regard to this point, there is a difference between the present

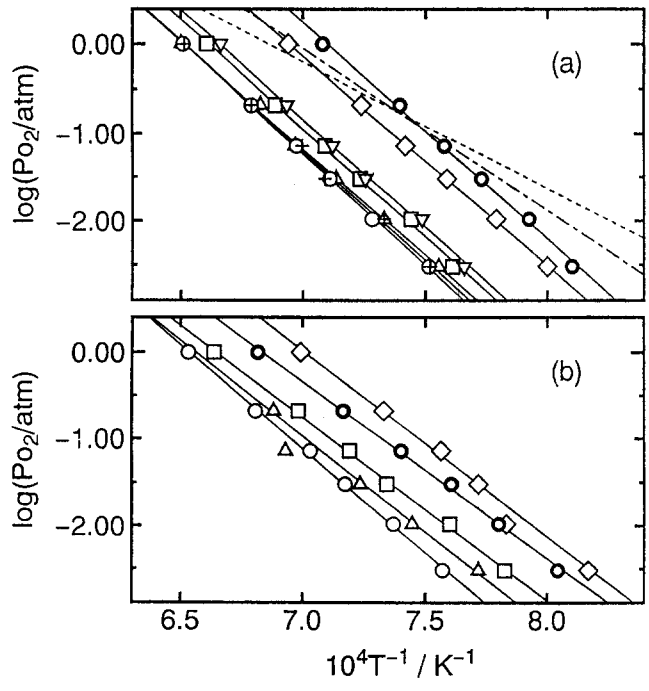

Fig. 3. Decomposition oxygen partial pressure vs. reciprocal temperature of $LnMn_2O_5$ obtained from DTA ($\log P_{O_2}$–$1/T$ phase diagrams): Gd; (a) ◎, Pr; □, Eu; ◇, Nd; △, Tb; ▽, Sm; ○, Gd; +, Dy; (b) ○, Ho, □, Er; ◎, Tm; ◇, Yb; △, Y; ——, results of least-squares method for each $LnMn_2O_5$; – – –, results for $PrMn_2O_5$ of Cherepanov et al. [13]; – · –, result for $NdMn_2O_5$ of Cherepanov et al. [13].

Table 3
Coefficients A and B of Eq. (1) calculated from differential thermal analysis and enthalpy and entropy changes at the mean temperature for decomposition of $LnMn_2O_5$

Specimen	A ($\times 10^4$ K^{-1})	B	T_{mean} (K)	ΔH° (kJ mol^{-1})	ΔS° (J mol^{-1} K^{-1})
$PrMn_2O_5$	2.371	16.81	1323	151.3	107.3
$NdMn_2O_5$	2.372	16.47	1346	151.4	105.1
$SmMn_2O_5$	2.463	16.40	1402	157.2	104.7
$EuMn_2O_5$	2.376	15.69	1414	151.6	100.1
$GdMn_2O_5$	2.539	16.54	1434	162.0	105.6
$TbMn_2O_5$	2.423	15.78	1431	154.6	100.7
$DyMn_2O_5$	2.485	16.21	1433	158.6	103.5
$HoMn_2O_5$	2.401	15.70	1426	153.2	100.2
$ErMn_2O_5$	2.120	14.09	1393	135.3	89.9
$TmMn_2O_5$	2.043	13.96	1355	130.4	89.1
$YbMn_2O_5$	2.147	15.05	1327	137.0	96.1
YMn_2O_5	2.212	14.52	1375	141.2	92.7

results and those of Cherepanov et al. [13]. Their lines showing the phase boundary in $\log P_{O_2}$–$1/T$ plot cross for $PrMn_2O_5$ and $NdMn_2O_5$. The stability is inverted near atmospheric pressure. However, the $NdMn_2O_5$ phase is always more stable in the present work than $PrMn_2O_5$ in all ranges of temperature and oxygen pressure in our results. $DyMnO_3$ is the most unstable phase among the perovskite phases (La–Dy), but $DyMn_2O_5$ is one of the most stable phases among $LnMn_2O_5$. So it is interesting that $PrMnO_3$ has the widest stable range about the stability of both phases, while $DyMnO_3$ has the smallest range.

The enthalpy and entropy changes that accompany the decomposition reaction were calculated and the results are tabulated in Table 3. Since standard enthalpies of formation and entropies for $LnMnO_3$ and Mn_3O_4 are known [14], those of $LnMn_2O_5$ at the mean temperature could be estimated, and they are tabulated in Table 4.

Table 4
Standard enthalpy changes of formation and entropies of $LnMn_2O_5$ at the mean temperature in the present measurement

Specimen	T_{mean} (K)	ΔH_f° (kJ mol^{-1})	S° (J mol^{-1} K^{-1})
$PrMn_2O_5$	1323	−2462.4	453.1
$NdMn_2O_5$	1346	−2037.1	456.5
$SmMn_2O_5$	1402	−2054.2	461.6
$EuMn_2O_5$	1414	−1948.3	469.3
$GdMn_2O_5$	1434	−2039.5	458.5
$TbMn_2O_5$	1431	−2048.2	470.7
$DyMn_2O_5$	1433	−2044.1	464.1
$HoMn_2O_5$	1426	−2052.2	467.1
$ErMn_2O_5$	1393	−2037.0	471.0
$TmMn_2O_5$	1355	−2019.3	459.6
$YbMn_2O_5$	1327	−1999.6	445.3
YMn_2O_5	1375	−2048.4	434.4

The reaction is

$$Ln(s) + 2Mn(s) + \tfrac{5}{2}O_2(g) \rightarrow LnMn_2O_5(s)$$

4. Conclusion

The stabilities of $LnMn_2O_5$ at high temperature were studied by DTA. The accuracy of measurement of 2% for the results from DTA was better than for TG. The most stable phases were $GdMn_2O_5$ and $DyMn_2O_5$, and the most unstable phase was $PrMn_2O_5$. All the $LnMnTiO_5$ were more stable than $GdMn_2O_5$. The decomposition reaction for each compound was confirmed.

On the basis of the reaction, the enthalpy and the entropy changes that accompanied the decomposition were obtained. For $LnMn_2O_5$ the standard enthalpy of formation and entropy were also estimated at the mean temperature.

Acknowledgment

The present work was supported by Grant-in-Aid for Scientific Research on Priority Areas "New Development of Rare Earth Complexes" 06241236 from the Ministry of Education, Science and Culture.

References

[1] S. Quezel-Ambrunaz, E.F. Bertaut and G. Buisson, *C.R. Acad Sci., 258* (1964) 3025–3028.
[2] G. Buisson, *J. Phys. Chem. Solids, 31* (1970) 1171.
[3] I. Yaeger, *Mater. Res. Bull., 13* (1978) 819.
[4] I. Yaeger, *J. Appl. Phys., 49* (1978) 1513.
[5] E.F. Bertaut, G. Buisson, A. Durif, A. Mareschal, M.C. Montmory and S. Quezel-Ambrunaz, *Bull. Soc. Chim. Fr.*, (1965) 1132–1137.
[6] S.C. Abrahams and J.L. Bernstein, *J. Chem. Phys., 46* (1967) 3776.
[7] B.M. Wanklyn, *J. Mater. Sci. A, 7* (1973) 813.
[8] G. Buisson, *Phys. Status Solidi A, 17* (1973) 191.
[9] P.P. Gardner, C. Wilkinson, J.B. Forsyth and B.M. Wanklyn, *J. Phys. C, 21* (1988) 5653.

[10] V.A. Sanina, L.M. Sapozhnikova, E.I. Golovenchits and N.V. Morozov, *Fiz. Tverd. Tela (Leningrad)*, *30* (1988) 3015 (*Sov. Phys. Solid State*, *30* (1989) 1736.
[11] P. Euzen, P. Leone, C. Gueho and P. Palvadeau, *Acta Crystallogr. C*, *49* (1993) 1875.
[12] G. Boisson, in J.P. Suchet (ed.), *Croissance de Composes Mineraux Monocristallins*, Masson, Paris, 1969.
[13] V.A. Cherepanov, L. Yu. Barkhatova and A.N. Petrov, *J. Phys. Chem. Solids*, *55* (1994) 229.
[14] Society of Calorimetry and Thermal Analysis, Japan, *Thermodynamic Data Base MALT2*, Kagakugijutsusha, 1992.
[15] H. Satoh, M. Horikawa and N. Kamegashira, *J. Alloys. Comp.*, *192* (1993) 99.
[16] H. Satoh, M. Horikawa and N. Kamegashira, *Netsu Sokutei*, *20* (1993) 193.
[17] H. Satoh, T. Shoji, J. Iwasaki and N. Kamegashira, *Thermochim. Acta*, to be published.
[18] H.W. Xu, J. Iwasaki, T. Shimizu, H. Satoh and N. Kamegashira, *J. Alloys Comp.*, *221* (1995) 274.
[19] W. DeSisto, N. Kamegashira, W.Y. Chang, M. Hart, J. Baglio, K. Dwight and A. Wold, in C.N.R. Rao (ed.), *Chemical and Structure Aspects of High Temperature Superconductivity*, Vol. 7, World Scientific, Singapore, 1988, p. 32.
[20] M.W. Chase, Jr., C.A. Davies, J.R. Downey, Jr., D.J. Frurip, R.A. McDonald and A.N. Syverud, *JANAF Thermodynamic Tables*, 3rd edn., in *J. Phys. Chem. Ref. Data*, *14* (Suppl. 1) (1985).